Phase Transition of Interstellar CO Ice

Jiao He[1] , Francis E. Toriello[2], Shahnewaz M. Emtiaz[2], Thomas Henning[1] , and Gianfranco Vidali[2]
[1] Max Planck Institute for Astronomy, Königstuhl 17, D-69117 Heidelberg, Germany; he@mpia.de
[2] Physics Department, Syracuse University, Syracuse, NY 13244, USA

Abstract

Among the over 200 molecular species identified in interstellar clouds, many are organic molecules. It has been proposed that some of these molecules survive the star and planet formation process and are eventually delivered to Earth where they can form the molecular basis of the origin of life. It is now well established that one of the most important factories of these molecules are ice mantles that cover the dust grains in star-forming molecular clouds. Simple atoms and molecules such as H, O, N, and CO condense from the gas phase onto the grain surface and then react with each other in the ice to form increasingly complex molecules. At the extremely low temperature (10–15 K) in these clouds, the widely accepted mechanism to bring reactive species together—diffusion—is severely impeded in the ice, raising the question of the mechanism of their formation. In laboratory experiments we find that the top layers of the ice mantle, which are made primarily of CO, transform from a disordered phase to a polycrystalline phase at such a low temperature. During the phase transition, reactive species buried inside may migrate and react without the need to overcome activation energy for diffusion. By quantifying the kinetics of crystallization, we predict that CO ice in interstellar clouds is mostly in the polycrystalline form. The reorganization of CO ice, which occurs below 10 K, may promote mobility of reactive species, and therefore can be a driving force of molecular complexity in molecular clouds.

1. Introduction

Dust grains in star-forming regions, the so-called dense molecular clouds, are covered by an ice mantle with an onion-like layered structure. The inner layer is mostly made of amorphous water ice and other minor components such as CO_2, NH_3, and CH_4, while the outer layer is dominated by CO (Pontoppidan et al. 2008; Boogert et al. 2015). A survey of dozens of young low-mass stellar objects found a CO ice abundance only second to water and CO_2. A comparison of the observed CO stretching infrared band in most lines of sight in young stellar objects (YSOs) with laboratory measurements show that 60%–90% of the solid CO is in a nearly pure form rather than in a water-rich environment (Pontoppidan et al. 2003; Boogert et al. 2015). This is likely the case in other dense cloud environments as well. Laboratory experiments and astrochemical models all suggest that many complex organic molecules (COMs; generally defined as organic molecules with six or more atoms in the astronomical community) are formed in the CO-rich layer (Chuang et al. 2017; Simons et al. 2020). H atom addition reactions in the CO-rich ice lead to the formation of simple molecules and radicals such as HCO, H_2CO, CH_2OH, CH_3O, and CH_3OH. The recombination reactions between HCO, CH_2OH, and CH_3O radicals further form methyl formate (CH_3OCHO), glycolaldehyde ($HOCH_2CHO$), and ethylene glycol (($CH_2OH)_2$), all of which have been detected in the interstellar space (Chuang et al. 2016; McGuire 2018). In addition to H and CO, other reactive species such as O and OH may also participate in the chemistry. It is the reactions between reactive species, especially radicals, that build up the molecular complexity in star formation regions.

Key to the formation of COMs in interstellar ices is the process of diffusion of reactants, which is generally assumed to be the main driving force to bring reactive species together to react. However, the activation energy of diffusion of molecules and radicals in ices is poorly known. Astrochemical models that simulate the chemical evolution of interstellar matter assume that the activation energy of diffusion is a fraction of the binding energy, although the value of this fraction is poorly constrained, with estimates ranging from 0.3 to 0.8 of the binding energy (Garrod & Herbst 2006; Ruaud et al. 2016; He et al. 2018b). At 10–15 K, which is the typical temperature in dense molecular clouds, the probability of overcoming a typical activation energy barrier is exceedingly small (Garrod & Herbst 2006), with the exception of hydrogen atoms and molecules. However, observations point to the formation of COMs in star-forming regions before the cloud is warmed by the nascent star (Bacmann et al. 2012; Cernicharo et al. 2012). The feasibility of COMs formation at this low temperature and without the aid of energetic particles/radiation has been demonstrated in the identification of two-carbon COMs in a laboratory experiment of H atom addition to CO ice at 10 K (Chuang et al. 2016). How atoms and radicals in the ice are brought together to react is an unsolved fundamental problem in astrochemistry.

It has been known for almost two decades that CO ice in YSOs is mostly in the pure form (Pontoppidan et al. 2003). However, the morphology (amorphous versus crystalline) of it has not been the focus of any previous study. As a comparison, the morphology of water ice, which is the other component of the ice mantle, has been studied extensively, both experimentally and theoretically (Essmann & Geiger 1995; Jenniskens & Blake 1996; May et al. 2012). As is known from previous studies, the phase transition of water ice is typically accompanied by the segregation and possible desorption of the impurities. Trapped gases in amorphous water ice are released through cracks that develop in the crystallization process. The eruption of volatiles during the crystallization is

called a "molecular volcano" (Smith et al. 1997). Molecules more volatile than water ice desorb during the molecular volcano, but less volatile molecules remain in a segregated form and desorb at higher temperatures. We decided to see whether a similar transition happens in CO ice, what is the temperature of the transition, and whether impurities segregate into clusters during the transition. If the impurities happen to be reactive, chemical reactions between them could form COMs. To verify it, laboratory experiments were performed under dense cloud relevant conditions to study the crystallization of CO ice, with and without impurities, on an amorphous solid water ice film that emulates the inner layers of the ice mantle.

2. Experimental Setup

Experiments were performed in an ultra-high vacuum (UHV) chamber with a base pressure 4×10^{-10} torr, located in the Laboratory of Astrophysics and Surface Science at Syracuse University. More detailed description of the apparatus and experimental protocols can be found in previous works (He et al. 2018a, 2018b; He & Vidali 2018). Here only the main features that are closely relevant to this study are summarized. Located at the center of the chamber is the substrate, which is a gold-coated copper disk attached to the cold finger of a closed-cycle helium cryostat (ARS DE-204 4K). The sample temperature is measured by a calibrated silicon diode sensor (Lakeshore DT-670) placed behind the substrate. A cartridge heater in the sample holder is used to heat the sample. A Lakeshore 336 temperature controller reads and controls the temperature between 5 and 300 K with an accuracy better than 50 mK. Ice on the gold surface is monitored by a Nicolet 6700 Fourier Transfer Infrared Spectrometer in the Reflection Absorption InfraRed Spectroscopy (RAIRS) configuration. The spectrometer scans between 650 and 4000 cm^{-1} at a spectral resolution of 1 cm^{-1}. A total of 16 scans are averaged every 20 s to increase the signal-to-noise ratio.

CO/CO_2 and water vapor are introduced into the chamber through two variable leak valves. Each leak valve is controlled by a stepper motor linked to a LabVIEW program. The deposition rate and ice thickness are calculated based on the impingement rate, which is the number of molecules colliding with the cold surface in unit time and on unit surface area (He et al. 2018a). The relative accuracy of the deposition rate is estimated to be better than 0.1% and 1% for CO and water, respectively.

In all experiments, 30 monolayer of water ice was grown on the gold surface when it was at 10 K. Afterward, the water ice was annealed at 130 K for at least one hour to make it compact and then cooled down to 6 K for further experiments. In experiments where a $CO:CO_2 = 9:1$ mixture was used, CO and CO_2 gases were pre-mixed in a separate 0.5 liter canister and then sent to the chamber through a leak valve. Due to the difference in pumping speed for CO and CO_2, the ice composition on the substrate may differ slightly from the gas composition in the canister. We ignore this small difference in the analysis and assume that the $CO:CO_2$ mixing ratio in the ice is 9:1. For each deposition of CO or $CO:CO_2$ mixture, the deposition duration was 2 minutes, regardless of the thickness. This relatively short deposition time ensures that negligible water vapor from the chamber background is condensed together with the CO or CO2.
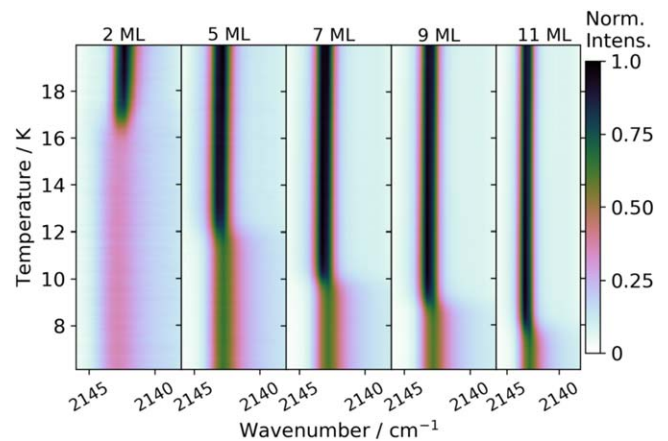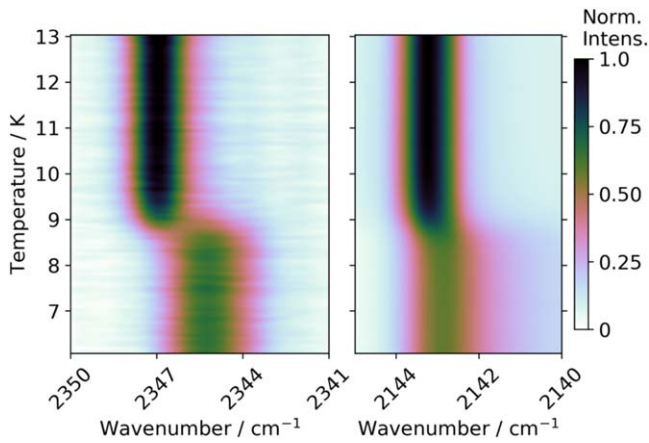

Figure 1. 2D plot of the RAIRS spectra measured during warm-up of CO ice of different thickness. The CO ices are deposited on top of np-ASW surface at 6 K and then warmed up at 0.2 K/minute. The ice thickness is marked on top of each column. The intensity is normalized to the maximum intensity reached in the warm-up.

3. Results and Analysis

In this study, CO ice was grown by background gas deposition on top of non-porous amorphous solid water (np-ASW) film at 6 K. After deposition, the ice was warmed up from 6 to 20 K at a ramp rate of 0.2 K/minute. Infrared spectra in the RAIRS configuration were measured during warm-up. Experiments were performed with different CO ice thickness, and the spectra are shown in Figure 1. In the RAIRS configuration, the longitudinal optical (LO) mode at $\sim$2143 cm^{-1} is much more pronounced than the transverse optical (TO) mode at $\sim$2138 cm^{-1}, and therefore our analysis is only based on the LO mode. Changes in both band shape and position of the LO mode are clearly seen for all thicknesses, indicating a structural change in the ice. As the thickness increases, the temperature of the structural change decreases. We attribute the structural change to a phase transition from an amorphous or orientationally disordered phase to a polycrystalline phase (Mizuno et al. 2016). Because the thickness of the CO ice investigated in this study as well as that on interstellar dust grains is small, the formation of an extended crystalline phase is likely to be hampered by the confined geometry, and the formation of polycrystals is more probable.

Under a realistic dense cloud condition, the CO-rich layer on dust grains likely contains impurities such as H, O, HCO, CO_2, etc. To investigate whether the crystallization of CO ice is accompanied by the segregation of impurities, we study the crystallization and segregation of a mixture of CO and CO_2 in the ratio 9:1. The prepared mixture was deposited on an np-ASW surface at 6 K, yielding a 10 monolayer (ML; defined as 10^{15} molecule per cm^2) ice. The ice was then warmed up at a ramp rate of 0.2 K/minute. Figure 2 shows the RAIRS spectra measured during the warm-up. Between 8 and 9 K, the CO absorption profile sharpens and the peak intensity increases, similarly to Figure 1. In the same temperature range, the asymmetric stretching (ν_3) peak of CO_2 blueshifts from 2344.9 to 2346.7 cm^{-1}. The former is representative of isolated CO_2 molecules while the latter is due to clusters of CO_2 molecules (He et al. 2017). Here we used CO_2 as a proxy of impurities present in the CO-rich layer of the ice mantle since CO_2 is also present in the ice mantle on dust grains (Gerakines et al. 1999; Pontoppidan et al. 2008). Other impurities should also

Figure 2. Same as in Figure 1 but for a 10 ML of a $CO:CO_2 = 9:1$ mixture.

Figure 3. Crystallization time (t_{crys}) as a function of CO ice thickness and temperature. The crystallization time is defined here as the time for the degree of crystallinity to reach half maximum. The time is represented in the logarithmic scale as $log_{10}(t_{crys}/year)$.

segregate similarly. The crystallization of the $CO:CO_2$ ice mixture occurs at a similar temperature as the pure CO ice of the same thickness (see Figure 1), suggesting that a small fraction of impurities does not affect the crystallization kinetics significantly and that the result on pure CO ice should apply to dense clouds conditions where impurities are present.

The experimental condition differs from dense clouds in the warm-up timescale. In the laboratory it is from minutes to hours, while in interstellar clouds it can be as long as thousands of years or even longer. Simple calculation are done to extrapolate the experimental results to the astronomical time-scale. Following the Johnson–Mehl–Avrami–Kolmogorov theory (Avrami 1941), we performed an analysis of the experimental results (see the Appendix), and found that the crystallization of CO ice can be described by the following empirical formulae:

$$Y = 1 - \exp(-k(T)t^n) \quad (1)$$

$$k(T) = \nu \exp(-E/T) \quad (2)$$

$$E = 443 \exp(-0.154\, d) + 200 \quad (3)$$

where Y ($0 < Y < 1$) is the degree of crystallinity, t is the time, $n = 0.8$ is the Avrami exponent, $k(T)$ is the crystallization rate constant, $\nu = 5.3 \times 10^9$ is the pre-exponential factor, E is the activation energy for crystallization, d is the thickness in ML, and T is the temperature. Here we followed the convention in astronomy to use Kelvin (K) as the energy unit. It can be converted to j mol^{-1} by multiplying the Boltzmann constant.

4. Astrophysical Applications

We apply the kinetics of CO phase transition to dense cloud conditions. Based on Equations (1)–(3) we calculate the crystallization time t_{crys}, which we define as the time it takes for the degree of crystallinity Y to reach half of its maximum value. The t_{crys} as a function of both ice thickness and temperature is shown in Figure 3. It is clear that except for the thinnest and coldest CO ice, crystallization should occur within the typical pre-stellar core lifetime 10^5 yr. Therefore, the majority of the CO ice in the top layers of the ice mantle is likely to be in the polycrystalline phase, and chemical reactions among reactive impurities should take place to form COMs during the crystallization instead of through diffusion at a later warm-up stage.
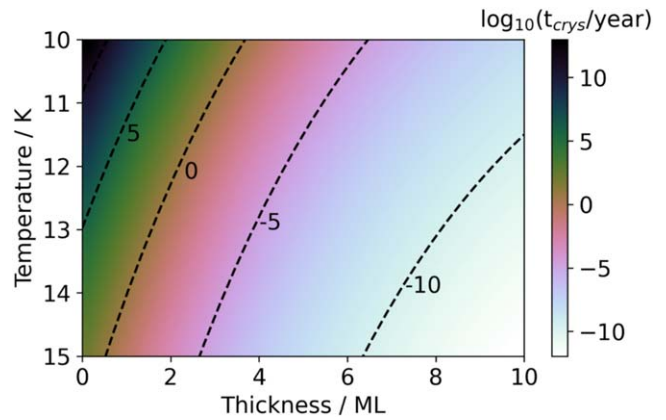
The above discussion assumed the simplest scenario, i.e., constant temperature and thickness, and that the phase transition of the CO ice is irreversible. However, the condition in dense clouds is more complicated and the above assumptions may not be true. The bombardment of cosmic rays causes temperature fluctuations, with smaller grains experiencing a larger temperature variation (Purcell 1976). The thickness of CO ice changes as well due to the continuous condensation of CO gas along with impurities, and perhaps also due to desorption of CO when temperature spikes. The morphology may change from polycrystalline to amorphous when ionizing irradiation breaks up molecules and creates new impurities. Subsequent crystallization once again drives the segregation of impurities and promotes the chemical reactions between them. Therefore, a dynamic process of ice growth and desorption, crystallization and amorphization, is likely to occur in the ice mantle. Chemical bonds are repeatedly broken and formed, and molecular complexity is increased along the way. This process is likely to be responsible for the formation of many COMs in the ice mantle.

In numerous laboratory experiments that simulate the energetic processing of the ice mantle, COMs are routinely identified, even at below 10 K (e.g., Abplanalp et al. 2015; Abplanalp & Kaiser 2019; Sandford et al. 2020). Because of the inefficiency of diffusion of radicals at low temperature, the formation of COMs is usually explained by the recombination of radicals that are nearby each other. Based on this study, we propose an alternative explanation that the COMs may have been formed by the segregation of radicals during the phase transition of the ice, considering that at the typical experimental temperature in those studies, the phase transition of a thick CO ice already proceeds rapidly. The processes of repetitive crystallization and amorphization might facilitate the formation of COMs during the whole irradiation stage. In this study, we investigated the phase transition of CO-dominated ice. In experiments with ices dominated by other molecules such as CH_4 or NH_3, it is possible that a similar mechanism exists to explain the formation of COMs and dedicated experiments need to be performed.

5. Discussions

The structure of CO ice is important for the chemistry on dust grains. However, it has largely been overlooked in

previous astronomical/astrochemical studies, including observations, computer modeling, and laboratory simulations. Future endeavors should combine efforts from all of the three aspects. In observations, comparing observed spectra with the laboratory spectra of CO of different morphologies would make it possible to confirm the structure of CO ice on dust grains, as it was done for water ice (Smith et al. 1989). In astrochemical models of the interstellar medium, it is crucial to take into account the phase transition of CO ice as a mechanism for solid-state reactions in addition to the conventional mechanism of thermal diffusion. This is especially important for well-shielded clouds where the dust grain temperature is too low for thermal diffusion to be efficient. Computational chemistry would also lend help in systematically studying how the crystallization depends on the substrate material, temperature, thickness, and composition of the ice. In the laboratory, at least three types of experiments would be highly valuable. First, infrared spectra of CO ice of different morphologies, with and without segregated impurities, need to be measured. The spectra of the impurities are likely to be affected by the morphology of CO ice and may provide a powerful tool to probe the physical environment of the ice mantle, and even provide an insight into the formation mechanism of molecules. Second, more experimental studies are needed to further constrain the crystallization kinetics of pure CO ice and CO ice with impurities. Infrared spectroscopy, which has been used in this study, should be paired with other techniques such as neutron scattering, X-ray diffraction, and reflection high-energy electron diffraction (RHEED), which are widely used to characterize the structure of molecular solids. RHEED would be particularly helpful as it has been successfully demonstrated in studies of thin ice films (Yang & Zewail 2009). They would certainly provide further insight into the structure of CO ice and crystallization kinetics (Souda & Aizawa 2019). Third, laboratory simulations of the chemistry in the ice mantle that take into account the thickness of the CO ice will be fruitful. In the last two decades, numerous laboratory studies of the chemistry in CO-containing ices have probed thermally activated and ionizing irradiation driven reactions (Bennett et al. 2010; Kim et al. 2011; Linnartz et al. 2015; Chuang et al. 2017; Abplanalp & Kaiser 2019; Eckhardt et al. 2019) without considering the role of the thickness. As discussed above, the radicals that are produced as a result of either thermal reactions or ionizing irradiations can segregate and react to form COMs. As is shown in Figure 1, the crystallization of CO ice strongly depends on its thickness. Experiments that utilizes a thicker CO ice, as in most existing laboratory studies, likely overestimated the yield of complex organic molecules. Further laboratory studies will help to better constrain the formation of COMs in interstellar clouds.

Data Availability

The experimental data for this work is stored on Zenodo under a Creative Commons Attribution license 10.5281/zenodo.4783316 .

Appendix
Kinetics of Crystallization

To obtain the kinetics of the crystallization and segregation, we performed a set of isotherm experiments of $CO:CO_2$ mixtures in the ratio 9:1. A total of 10 ML was deposited onto an np-ASW surface at 6 K. Afterward, the ice was heated up at a high ramp rate of 12 K/minute to a target temperature between 7.9 and 8.8 K, and remained at this temperature for at least one hour; RAIRS spectra were measured continuously. As an illustration, Figure 4(a) shows the CO_2 ν_3 band of the RAIRS spectra at a few selected times during the isotherm at 8.8 K. The CO_2 absorption band at the beginning of the isotherm shows a Gaussian line shape centered at 2344.9 cm^{-1}, but gradually shifts to a Lorentzian line shape centered at 2346.7 cm^{-1}. The peak at 2344.9 cm^{-1} is representative of low concentration or isolated CO_2 molecules, while the blueshifted peak at 2346.7 cm^{-1} is due to segregated CO_2 in the form of clusters (He et al. 2017). We decompose the CO_2 absorption band in each spectra using one Gaussian function centered at 2344.9 cm^{-1} and one Lorentzian function centered at 2346.7 cm^{-1}. The fittings of the selected spectra are shown in Figure 4(a). In Figure 4(b), the time evolution of both band areas at different isotherm temperatures is shown. At all isotherm temperatures, the shift of peak position from 2344.9 to 2346.7 cm^{-1} is observed, and the rate of shifting depends on the temperature. We can also see that in all these measurements, before the annealing, the CO_2 absorption is dominated by the 2344.9 cm^{-1} band, indicating that the ice upon deposition has a very low degree of crystallinity. This suggests that the 300 K kinetic energy from gas is not affecting the initial structure of the ice.

We use the Johnson–Mehl–Avrami–Kolmogorov equation, or simply the Avrami equation (Avrami 1939, 1940, 1941), to describe the kinetics of crystallization.

$$Y = 1 - \exp(-kt^n) \tag{A1}$$

where Y is the degree of crystallinity, n is the Avrami exponent, and k is the crystallization rate constant. To obtain the value of n, we plot $\ln(-\ln(1 - Y))$ versus $\ln(t)$ in Figure 5(a). Here the value of Y is obtained from Figure 4(b). We assume that when the band area for the 2344.9 cm^{-1} is zero, the value of Y is 1. The slope of the curves in Figure 5(a), which is the value of the Avrami exponent n, is found to be about 0.8. In later calculations, we use the value $n = 0.8$ to analyze the crystallization kinetics for both pure CO ice and CO:CO2 mixtures.

In the conventional theory of crystallization, the n value for a three-dimensional solid is usually between 3 and 4. However, in a geometrically confined solid, lower values are possible. The n value for ASW has been found to decrease from 4 to about 1 when the thickness of ice decreases from 18 to about 5 ML (Harada et al. 2020). Another study found that the n value of 100 nm of ASW decreases from 2.17 to 1.0 when the ice growth temperature drops from 90 K to 14 K (Maté et al. 2012). Because the CO ices in our experiments are grown at an even lower temperature 6 K, and the thickness is much smaller, the low value $n = 0.8$ is reasonable. Based on the Avrami equation, one can see that compared with $n = 3$, the smaller value $n = 0.8$ would mean that it takes much longer time to reach a full crystallization state. Given the very low temperature and very confined geometry at the thickness explored, this is not surprising. Nonetheless, we believe that the n value may

(a)

(b)
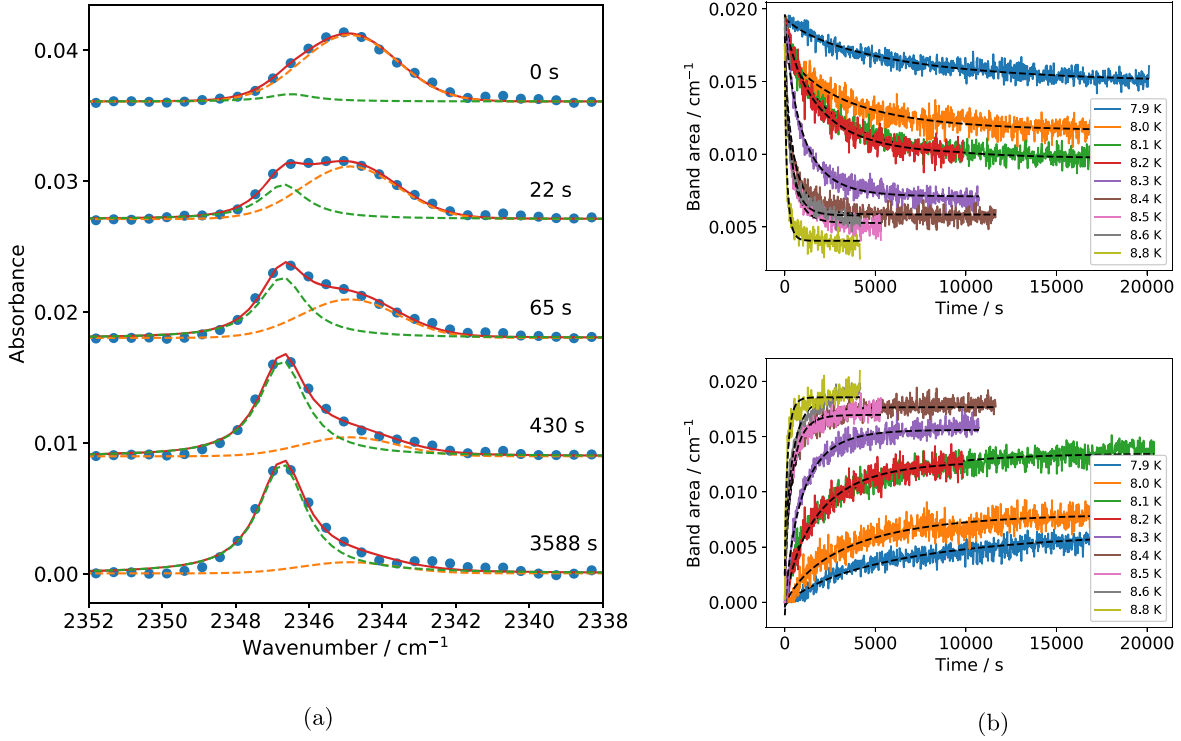
Figure 4. (a) RAIRS of 10 ML of a CO:CO_2 9:1 mixture deposited on np-ASW at 6 K and then warmed to 8.8 K for isothermal processing. Different curves show the spectra after various times of isothermal processing. The CO_2 absorption profile (blue circles) is fitted with a Gaussian function centered at 2344.9 cm^{-1} (orange dashed line) and a Lorentzian function centered at 2346.7 cm^{-1} (green dashed line). The total fitting is the red solid line. (b) Area of the CO_2 2344.9 cm^{-1} (top) and CO_2 2346.7 cm^{-1} (bottom) bands during isotherm experiments at the temperature indicated in the inset. The fitting using Area $= a \exp(-k(t - t_0)^{0.8}) + b$ is shown in black dashed lines.

depend on the thickness and the composition of the ice, and using a single value for all our experiments is only an estimation. Future experimental and theoretical studies of the CO ice crystallization would provide further constraints to this problem.

We used the equation

$$\text{Area} = a \exp(-k(t - t_0)^{0.8}) + b \qquad \text{(A2)}$$

to fit each curve in Figure 4(b), and obtain the k values at each temperature. An offset in time t_0 is introduced to account for the inaccuracy in determining the starting point of the isotherm experiments. The temperature dependence of the crystallization rate constant k can be described by Equation (2). Figure 5(b) shows the Arrhenius-type plot of the crystallization rate constant k, from which the values of ν and E were found to be 5.3×10^9 $s^{-0.8}$ and 231 K, respectively.

The above parameters should suffice to describe the crystallization of 9 ML of CO ice. Now we extend the analysis to other thicknesses as well. Ideally, one should carry out similar isotherm experiments for all CO thicknesses and derive the values of n, ν, and E for all thicknesses. Unfortunately, a detailed study is very time-consuming and out of the scope of this study. Instead, we take a simpler approach to assume that the values of n and ν are independent of the CO ice thickness, and only E changes with thickness. We denote it as E_d. Based on Figure 1 and other experiments in the same series but not shown in Figure 1, the crystallization temperature of various thicknesses of pure CO ice is obtained, which is shown in Figure 5(c). Also shown is the fitting using the formula of the form $T_{\text{crys}} = a \exp(-b\,d) + c$, where d is the thickness of CO

ice in ML. The best-fitting is

$$T_{\text{crys}} = 16.5 \exp(-0.20\,d) + 6.0. \qquad \text{(A3)}$$

In the slow warm-up experiments, the temperature follows a ramp of $\beta = 0.2$ K/minute.

$$T(t) = T_0 + \beta t \qquad \text{(A4)}$$

where $T_0 = 6$ K, and t is the time since the beginning of the warm-up. This crystallization process can be simulated by the Avrami equation, giving the values of n, ν, and various E_d values. Because Avrami equation is only applicable to the crystallization at a constant temperature, in our numerical computation, we make the temperature discrete. The ramp between 6 and 26 K is divided into 600 constant temperature mini-steps with a temperature interval of 0.033 K between them. Each step lasts for 10 s in which the Avrami equation is applicable. Different activation energy values between 200 and 550 K are plugged into Equation (2) to calculate the k value and subsequently plugged into Equation (1) to calculate the Y value. In this way, the degree of crystallinity Y as a function of temperature for different E_d values is calculated numerically and is shown in Figure 5(d). We take the temperature at which the Y value reaches half maximum to be the crystallization temperature T_{crys}, and in Figure 5(e) we plotted the T_{crys} versus the activation energy E_d, which follows a linear relation

$$T_{\text{crys}} = 0.0366 E_d + 0.319. \qquad \text{(A5)}$$

Combining Equations (A3) and (A5), we obtain the thickness-dependent activation energy as in Equation (3).

5

(a)

(b)

(c)

(d)

(e)
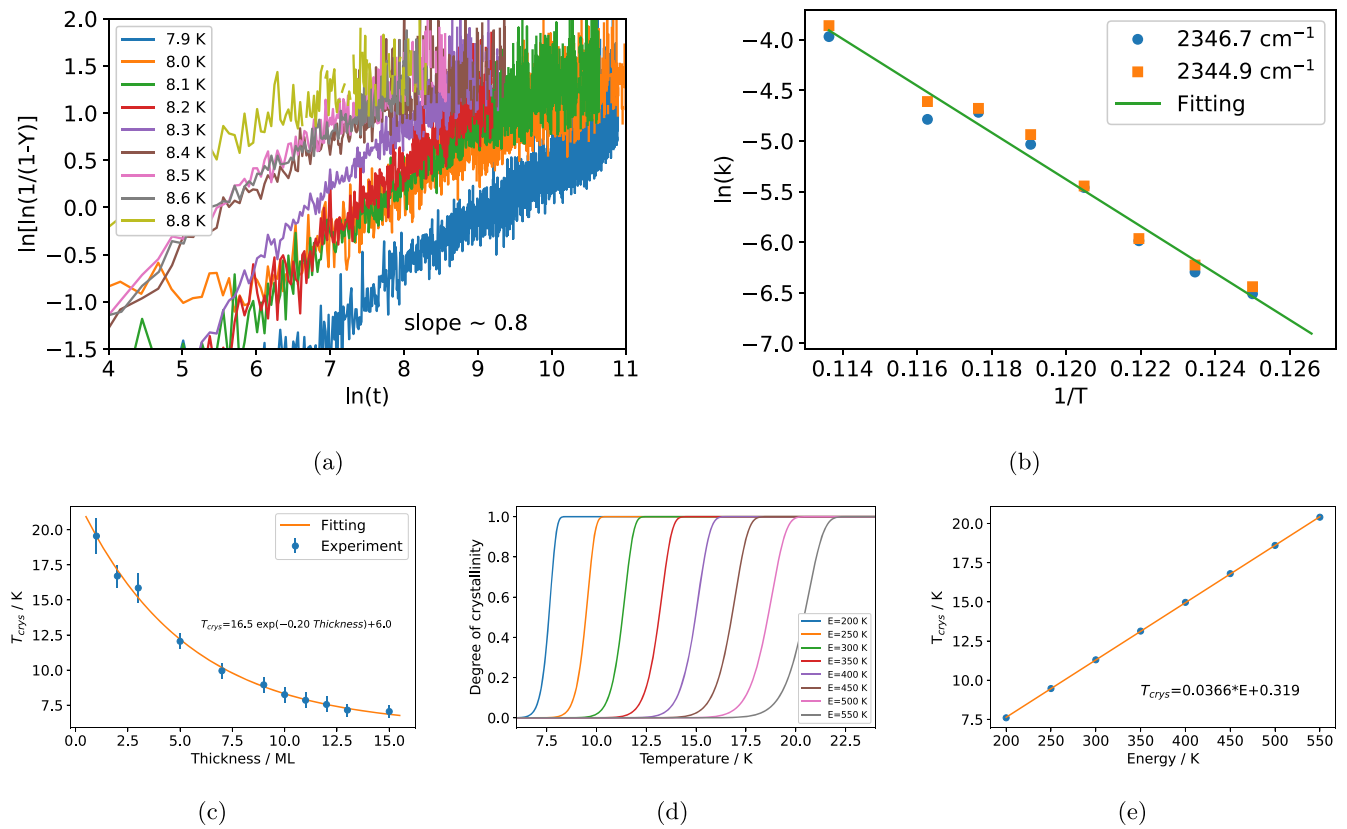
Figure 5. (a) $\ln(-\ln(1-Y))$ vs. $\ln(t)$, where Y is the degree of crystallinity. (b) Arrhenius plot of the crystallization constant $k(T)$ calculated from the 2344.9 cm^{-1} and 2346.7 cm^{-1} components. The linear fitting is shown with a green line. (c) The crystallization temperature of CO ice vs. the thickness (blue circles) and the fitting with an empirical function (orange line). The CO ices were grown on np-ASW at 6 K and then warmed up at a ramp rate of 0.2 K/minute. (d) Simulated degree of crystallinity vs. temperature using Avrami equation and assuming different activation energies for crystallization. The heating ramp rate is 0.2 K/minute. (e) Crystallization temperature vs. activation energy extracted from Figure 5(d). A linear fitting is shown with the orange line.

ORCID iDs

Jiao He ⬡ https://orcid.org/0000-0003-2382-083X
Thomas Henning ⬡ https://orcid.org/0000-0002-1493-300X
Gianfranco Vidali ⬡ https://orcid.org/0000-0002-4588-1417

References

Abplanalp, M. J., Borsuk, A., Jones, B. M., & Kaiser, R. I. 2015, ApJ, 814, 45
Abplanalp, M. J., & Kaiser, R. I. 2019, PCCP, 21, 16949
Avrami, M. 1939, JChPh, 7, 1103
Avrami, M. 1940, JChPh, 8, 212
Avrami, M. 1941, JChPh, 9, 177
Bacmann, A., Taquet, V., Faure, A., Kahane, C., & Ceccarelli, C. 2012, A&A, 541, L12
Bennett, C. J., Jamieson, C. S., & Kaiser, R. I. 2010, PCCP, 12, 4032
Boogert, A. A., Gerakines, P. A., & Whittet, D. C. 2015, ARA&A, 53, 541
Cernicharo, J., Marcelino, N., Roueff, E., et al. 2012, ApJ, 759, L43
Chuang, K.-J., Fedoseev, G., Ioppolo, S., van Dishoeck, E. F., & Linnartz, H. 2016, MNRAS, 455, 1702
Chuang, K.-J., Fedoseev, G., Qasim, D., et al. 2017, MNRAS, 467, 2552
Eckhardt, A. K., Bergantini, A., Singh, S. K., Schreiner, P. R., & Kaiser, R. I. 2019, Angew. Chem. Int. ed., 58, 5663
Essmann, U., & Geiger, A. 1995, JChPh, 103, 4678
Garrod, R. T., & Herbst, E. 2006, A&A, 457, 927

Gerakines, P. A., Whittet, D. C. B., Ehrenfreund, P., et al. 1999, ApJ, 522, 357
Harada, K., Sugimoto, T., Kato, F., Watanabe, K., & Matsumoto, Y. 2020, PCCP, 22, 1963
He, J., Emtiaz, S., Boogert, A., & Vidali, G. 2018a, ApJ, 869, 41
He, J., Emtiaz, S., & Vidali, G. 2018b, ApJ, 863, 156
He, J., Emtiaz, S. M., & Vidali, G. 2017, ApJ, 837, 65
He, J., & Vidali, G. 2018, MNRAS, 473, 860
Jenniskens, P., & Blake, D. F. 1996, ApJ, 473, 1104
Kim, Y. S., Zhang, F., & Kaiser, R. I. 2011, PCCP, 13, 15766
Linnartz, H., Ioppolo, S., & Fedoseev, G. 2015, IRPC, 34, 205
Maté, B., Rodríguez-Lazcano, Y., & Herrero, V. J. 2012, PCCP, 14, 10595
May, R. A., Smith, R. S., & Kay, B. D. 2012, J. Phys. Chem. Lett., 3, 327
McGuire, B. A. 2018, ApJS, 239, 17
Mizuno, Y., Kofu, M., & Yamamuro, O. 2016, JPSJ, 85, 124602
Pontoppidan, K. M., Boogert, A. C. A., Fraser, H. J., et al. 2008, ApJ, 678, 1005
Pontoppidan, K. M., Fraser, H. J., Dartois, E., et al. 2003, A&A, 408, 981
Purcell, E. M. 1976, ApJ, 206, 685
Ruaud, M., Wakelam, V., & Hersant, F. 2016, MNRAS, 459, 3756
Sandford, S. A., Nuevo, M., Bera, P. P., & Lee, T. J. 2020, ChRv, 120, 4616
Simons, M. a. J., Lamberts, T., & Cuppen, H. M. 2020, A&A, 634, A52
Smith, R. G., Sellgren, K., & Tokunaga, A. T. 1989, ApJ, 344, 413
Smith, R. S., Huang, C., Wong, E. K. L., & Kay, B. D. 1997, PhRvL, 79, 909
Souda, R., & Aizawa, T. 2019, PCCP, 21, 1123
Yang, D.-S., & Zewail, A. H. 2009, PNAS, 106, 4122